Geophysical Research Letters

RESEARCH LETTER
10.1029/2019GL085545

Intermodel Spread in the Northern Hemisphere Stratospheric Polar Vortex Response to Climate Change in the CMIP5 Models

Yutian Wu[1], **Isla R. Simpson**[2], **and Richard Seager**[1]

[1]Lamont-Doherty Earth Observatory, Columbia University, Palisades, NY, USA, [2]Climate and Global Dynamics Laboratory, National Center for Atmospheric Research, Boulder, CO, USA

Key Points:
- Resolved stationary wave driving accounts for less than 30% of the intermodel spread in the stratospheric polar vortex change in CMIP5
- Both altered vertical wave propagation into the stratosphere and altered meridional propagation within the stratosphere contribute
- Proposed theories for the stratospheric polar vortex response to climate change appear inadequate to explain the intermodel spread in CMIP5

Supporting Information:
- Supporting Information S1

Correspondence to:
Y. Wu,
yutianwu@ldeo.columbia.edu

Citation:
Wu, Y., Simpson, I. R., & Seager, R. (2019). Intermodel spread in the Northern Hemisphere stratospheric polar vortex response to climate change in the CMIP5 models. *Geophysical Research Letters*, *46*. https://doi.org/10.1029/2019GL085545

Received 24 SEP 2019
Accepted 29 OCT 2019
Accepted article online 9 NOV 2019

Abstract This study investigates the intermodel spread of the Northern Hemisphere winter stratospheric polar vortex change to anthropogenic greenhouse gas increase in Coupled Model Intercomparison Project Phase 5 (CMIP5) models. Previous proposed mechanisms for the polar vortex response to climate change, based on analysis of atmosphere-only models, are found inadequate to explain the intermodel spread in the coupled models in CMIP5. It is further found that resolved stationary wave driving in the polar vortex region accounts for less than 30% of the intermodel spread, and intermodel differences in both the vertical and meridional wave propagation contribute to differences in the wave driving. The results call for a detailed budget analysis of the stratospheric circulation response by including both the resolved and parameterized processes through the Dynamics and Variability Model Intercomparison Project. The results also highlight a need for an improved theoretical understanding of future projected polar vortex change and intermodel spread.

Plain Language Summary It has been increasingly recognized that the stratospheric circulation can significantly affect the troposphere and the surface through a downward influence, and thus, it is important to predict and understand how the stratospheric circulation will respond to anthropogenic greenhouse gas increase. However, there is a large disagreement in the stratospheric circulation response to climate change among the current generation of climate models. This study determines that previously proposed mechanisms to explain the intermodel spread are inadequate and, therefore, motivates an improved understanding of the stratospheric circulation response and model-to-model differences. This is a goal that should be achieved through forthcoming model intercomparison efforts.

1. Introduction

It is important to understand the future response of the Northern Hemisphere stratospheric polar vortex to anthropogenic greenhouse gas increase. It has been widely recognized that the stratospheric circulation can affect the troposphere and the surface through a downward influence on various time scales (e.g., Gerber et al., 2012; Kidston et al., 2015). On the climate change time scale, Manzini et al. (2014) performed linear regression analysis, based on a number of Coupled Model Intercomparison Project Phase 5 (CMIP5) models under the Representative Concentration Pathway 8.5 (RCP8.5) scenario, and found that models that simulate a greater weakening of the northern winter stratospheric polar vortex tend to exhibit less of a reduction in Arctic sea level pressure and less of a poleward shift in the Northern Hemisphere mid-latitude jet stream. Simpson et al. (2018) complemented this regression analysis by performing model experiments and imposing, by nudging, the extreme ends of CMIP5 stratospheric polar vortex change in a General Circulation Model (GCM). These model experiments explicitly demonstrated the cause-and-effect relationship between the stratospheric polar vortex change and tropospheric and surface change and confirmed the results found in Manzini et al. (2014). Simpson et al. (2018) also estimated that eliminating the uncertainty in stratospheric polar vortex change could help reduce the CMIP5 intermodel spread in Arctic sea level pressure projections by roughly 15–20% and noted the substantial difference in Mediterranean precipitation projections between models with polar vortex states on opposite ends of the distribution (see also Zappa & Shepherd, 2017).

While previous studies have demonstrated the large intermodel spread in the stratospheric polar vortex response to an increase of anthropogenic greenhouse gases (e.g., Manzini et al., 2014; Scaife et al., 2012; Shindell et al., 1999; Simpson et al., 2018), the underlying reason for this intermodel spread is not yet well understood. However, two dynamical mechanisms for the stratospheric polar vortex response to climate change and model-to-model differences have been proposed. One mechanism, proposed by Sigmond & Scinocca, 2010 (2010 hereafter SS2010), emphasizes the influence of the climatological, present-day, basic state and the influence that has on future change in *horizontal* wave propagation. They compared two versions of the Canadian Centre for Climate Modeling and Analysis Atmospheric GCM and found a strengthening of the stratospheric polar vortex in response to CO_2 doubling in one model version and a weakening in the other. The sea surface temperature (SST) fields in their doubling CO_2 experiments were taken from coupled simulations at the time of CO_2 doubling. They attributed the different polar vortex responses to differences in climatological zonal mean zonal winds in the lower stratosphere. They argued that the model with a stronger climatological lower stratospheric zonal wind had a smaller region of wave evanescence (characterized by negative refractive index) in the region linking the tropospheric and stratospheric westerlies, and the strengthening of the subtropical westerlies accompanying increasing CO_2 could, therefore, more easily lead to disappearance of the region of wave evanescence and thus an increase in equatorward wave propagation away from the polar vortex and an associated stratospheric polar vortex strengthening. The other mechanism, proposed by Karpechko & Manzini (2017, hereafter KM2017), argues for a change in tropospheric stationary waves and resulting changes in *vertical* wave propagation from the troposphere to the stratosphere. This mechanism was proposed based on analysis of an ensemble of Atmospheric Model Intercomparison Project (AMIP) experiments with prescribed SSTs. Within this ensemble, KM2017 found a robust Arctic stratosphere warming under increased SST scenarios. They argued that the subtropical jet strengthening that occurs with global warming leads to enhanced stationary wave activity, in particular a deepening of the climatological North Pacific low, and thus increased wave propagation from the troposphere into the stratosphere. They also found a significant negative correlation between the North Pacific low anomalies and the Arctic stratosphere temperature anomalies; that is, models with a larger deepening of the North Pacific low tend to have a larger Arctic stratosphere warming, accompanied by a greater polar vortex weakening. However, both SS2010 and KM2017 compared prescribed SST experiments so the SST changes were identical in each model and the climate sensitivities were similar and neither included any sea ice changes. Therefore, it still remains unclear whether these two prevailing mechanisms can explain results in the large number of CMIP5 models that have more realistic model setups with atmosphere-ocean-sea ice coupling as well as the other forcings present within the RCP8.5 scenario.

Therefore, in this paper, we discuss the dynamical mechanisms underlying the intermodel spread in the northern winter stratospheric polar vortex response to climate change in the coupled CMIP5 simulations under RCP8.5 forcing. We find that neither the SS2010 nor KM2017 mechanism is able to explain the intermodel spread in the coupled CMIP5 models. We further find that the difference in future changes in resolved stationary wave driving in the polar vortex region only accounts for less than 30% of the intermodel spread of the stratospheric polar vortex across 35 coupled CMIP5 models and differences in both vertical wave propagation and horizontal wave propagation play a role. The results point to the complex dynamical processes, including the responses in both resolved and parameterized processes, involved in the fully coupled CMIP5 simulation, and the need for an improved understanding of them.

2. Methods and Data

We use monthly output of zonal and meridional wind, temperature, and geopotential height from both the historical and RCP8.5 scenarios from 35 CMIP5 models. The anthropogenic climate change response is calculated as the difference between the RCP8.5 simulations from 2070–2099 and the historical simulations from 1979–2005. All available ensemble members for the historical and RCP8.5 scenarios (see supporting information) are used to minimize the role played by internal variability. The model outputs are regridded to a common 2° longitude by 2° latitude grid before the analyses are performed. We also make use of 6-hourly model-level output from 14 of the CMIP5 models (see supporting information). We present most of the results using monthly pressure-level output from the 35-model ensemble unless stated otherwise.

We quantify the strength of the stratospheric polar vortex using the zonal mean zonal wind at 10 hPa, averaged between 60°N and 75°N, following Simpson et al. (2018). As found in Simpson et al. (2018), this index

encompasses the region of the largest intermodel spread. We then calculate the future change in the stratospheric polar vortex averaged during January-February-March (JFM) and divide the CMIP5 models into a polar vortex weakening group (20 models) and a polar vortex strengthening group (15 models) determined by whether the change in strength of the stratospheric polar vortex is negative or positive, respectively. Climate sensitivity is found to have a negligible contribution in the grouping of the models and is barely correlated with the stratospheric polar vortex change across the models (not shown; see Figures 1e and 1f of Simpson et al., 2018).

The quasi-geostrophic Eliassen-Palm (E-P) flux diagnostics (Edmon et al., 1980) are used to quantify changes in wave activity. The E-P flux is composed of meridional (F_ϕ) and vertical (F_p) components, defined as follows:

$$\vec{F} = [F_{(\phi)}, F_{(p)}], \tag{1}$$

$$F_{(\phi)} = -a\cos\phi\langle u^* v^*\rangle, \tag{2}$$

$$F_{(p)} = af\cos\phi\frac{\langle v^*\theta^*\rangle}{\langle\theta\rangle_p}, \tag{3}$$

where ϕ is latitude, p is pressure, a is the Earth's radius, f is the Coriolis parameter, θ is potential temperature, u and v are the zonal and meridional wind velocities, angle brackets denote zonal average, and asterisks denote deviation from zonal average. The direction of the flux vectors provides an indication of the propagation of wave activity and the flux divergence, calculated as

$$\frac{1}{a\cos\phi}\nabla\cdot\vec{F} = \frac{1}{a\cos\phi}\left(\frac{1}{a\cos\phi}\frac{\partial F_{(\phi)}\cos\phi}{\partial\phi} + \frac{\partial F_{(p)}}{\partial p}\right), \tag{4}$$

measures the wave forcing on the zonal mean flow. We calculate the change in the E-P flux budget over a stratospheric region following previous studies (e.g., Hu & Tung, 2002; Kushner & Polvani, 2004; Sigmond & Scinocca, 2010). The E-P flux convergence in the stratospheric region bounded by latitudes ϕ_1, ϕ_2 and pressure levels p_1, p_2 can be written as

$$\begin{aligned}&\int_{p_1}^{p_2}\int_{\phi_1}^{\phi_2}\nabla\cdot\vec{F}\cos\phi\mathrm{d}\phi\mathrm{d}p\\ &= \int_{\phi_1}^{\phi_2}\cos\phi F_{(p)}\mathrm{d}\phi|_{p_2} - \int_{\phi_1}^{\phi_2}\cos\phi F_{(p)}\mathrm{d}\phi|_{p_1} + \frac{1}{a}\cos\phi\int_{p_1}^{p_2}F_{(\phi)}\mathrm{d}p|_{\phi_2} - \frac{1}{a}\cos\phi\int_{p_1}^{p_2}F_{(\phi)}\mathrm{d}p|_{\phi_1}.\end{aligned} \tag{5}$$

In this study we choose the stratospheric region as 55–90°N and 10–100 hPa. This is because this region encompasses the polar vortex weakening region in the weakening group (Figure 3a) and 10 hPa is the highest level where monthly model outputs are available for most models. The third term on the right-hand side of equation (5) also vanishes at 90°N.

3. Results

3.1. Stratospheric Polar Vortex Change in CMIP5 Coupled Simulations

Figure 1 shows the month-by-month evolution of the stratospheric polar vortex change for the weakening group and the strengthening group. It can be seen that the change is quite flat throughout the year in the strengthening group while it shows a pronounced deceleration during JFM for the weakening group. Since the multimodel mean difference between the two groups is the largest during JFM, we focus on the average over these three months. It is noted that this result is not sensitive to whether the grouping is made using the polar vortex change during JFM or the winter season as a whole (October–April).

3.2. Examination of Previous Hypotheses in CMIP5 Coupled Simulations

As described in section 1, two previous studies examined the model-to-model differences in future stratospheric polar vortex change—while KM2017 analyzed an ensemble of AMIP experiments and found the dominance of the stationary wave response, particularly over the northeastern Pacific, SS2010 studied two versions of a single comprehensive Atmospheric GCM and found the critical role of the region of wave

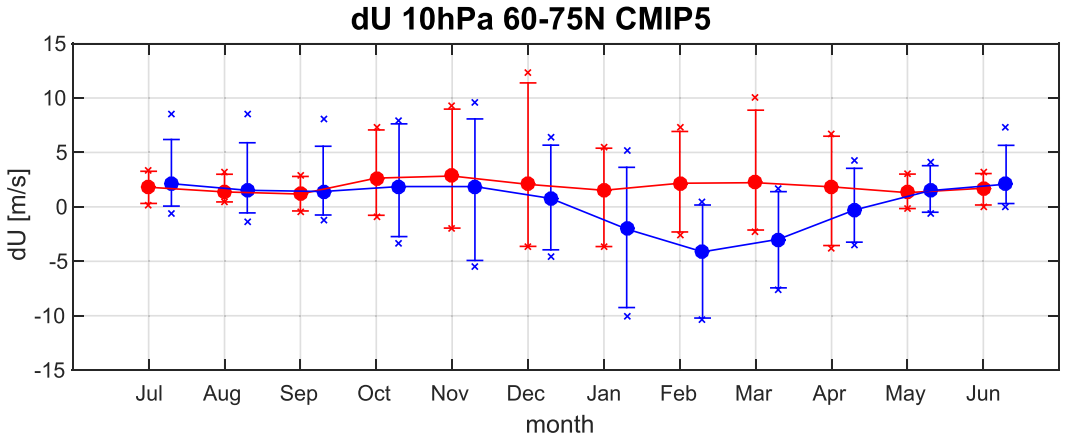

Figure 1. The CMIP5 stratospheric polar vortex change (RCP8.5 minus historical) month by month. The blue symbols denote the polar vortex weakening group (20 models) and the red the polar vortex strengthening group (15 models). The bars denote the 5th to 95th percentile range of the multimodel spread, the filled circles denote the mean value, and the diagnonal crosses denote the models outside of the 5th to 95th percentile range.

evanescence and its impact on equatorward wave propagation. Here, we first examine these two hypotheses in the coupled CMIP5 experiments.

Figures 2a and 2b test the KM2017 hypothesis in the coupled CMIP5 simulations. Figure 2a shows the multimodel mean change in 500 hPa eddy geopotential height and the difference in the multimodel mean change between the weakening and strengthening groups during December-January-February (DJF). A 1-month lag is introduced to focus on the wave drag conditions prior to JFM stratospheric polar vortex change. The conclusions remain the same with JFM wave drag conditions (not shown). Consistent with KM2017, a wave train response from East Asia across the North Pacific Ocean and North America toward Eurasia is seen in the multimodel mean, leading to a strengthened low in the northeastern Pacific. However, the difference between the weakening and strengthening groups is not statistically significant over the northeastern Pacific. Instead, a significant difference in geopotential height change is seen over the North Atlantic. Figure 2b is similar to Figure 9a of KM2017 and shows the relationship between the 500 hPa eddy geopotential height change averaged over the northeastern Pacific and the stratospheric polar vortex change (although here we use the vortex strength as opposed to polar cap temperature as a measure of the stratospheric change, but the results are largely similar with the polar cap temperature). A small and insignificant correlation is found between these two quantities across the coupled CMIP5 models and contrasts with the results of KM2017, in which a correlation coefficient of −0.79 is found in their 12-model AMIP4 K ensemble (see their Figure 9a) and −0.56 for the AMIPFuture scenario (see their Figure 9b). We randomly subsample 12 models from our 35-member ensemble, repeat this 10,000 times and find the probability of obtaining a correlation of −0.79 only 0.05% and the probability of obtaining a correlation of −0.56 only 1.25%. This likely points to a clear difference in the dynamical processes involved in the coupled model spread compared to those in AMIP and that the KM2017 conclusions drawn from prescribed SST AMIP runs are not necessarily applicable to explaining the intermodel spread in the fully coupled simulations.

In addition, Figures 2c–2f test the SS2010 hypothesis in the coupled CMIP5 ensemble. Panels (c) and (d) show the multimodel mean climatological zonal mean zonal wind and linear refractive index, and the difference between the weakening and strengthening groups. The linear refractive index is calculated as $n^2_{\text{ref}} = \frac{a\langle q_\phi \rangle}{\langle u \rangle - C_p} - \frac{k^2}{\cos^2\phi} - \frac{f^2 a^2}{4N^2 H_0^2}$, where q_ϕ is the meridional gradient of potential vorticity, C_p is the phase speed, k is the zonal wave number, N is the static stability, and $H_0 = 7$ km. Similar to SS2010, we choose $k = 0$ and $C_p = 0$ m/s. In contrast to SS2010, as shown in panels (c) and (d), neither a weaker climatological stratospheric polar vortex nor a larger area of negative climatological refractive index is found in the weakening group compared to the strengthening one. Rather, the weakening group compared to the strengthening one is associated with a statistically significantly stronger climatological jet on the equatorward flank of the stratospheric polar vortex and on the poleward flank of the tropospheric jet (Figure 2c). We notice that our Figure 2c differs from Figure 11b of Manzini et al. (2014) in that the latter study found a weaker climatological westerly wind in the subtropical lower stratosphere for the stratospheric polar vortex weakening models.

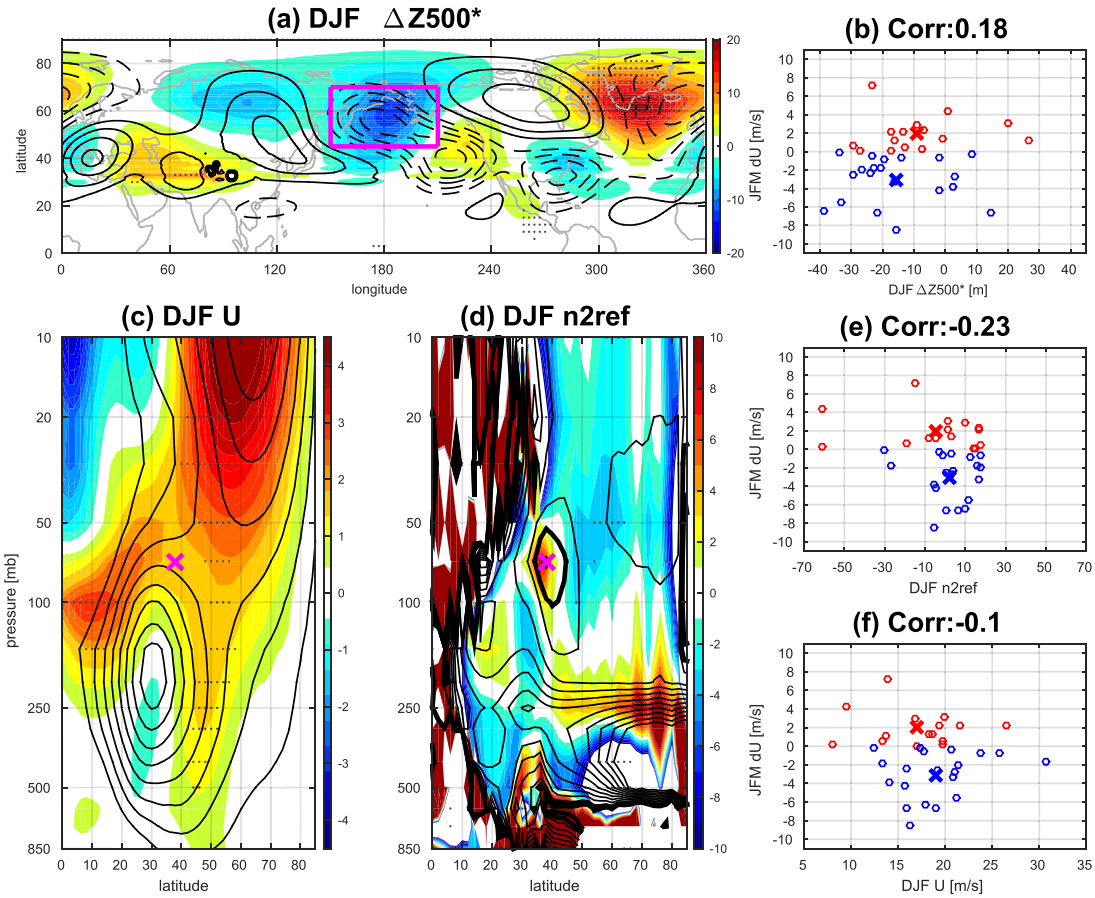

Figure 2. (a) Multimodel mean change in DJF 500 hPa eddy geopotential height (contours, contour interval = 5 m) and difference in multimodel mean change between the weakening group and strengthening group (color shadings). (b) Scatter plot of the JFM change in the stratospheric polar vortex strength versus DJF change in 500 hPa eddy geopotential height averaged over 150–210°E and 45–70°N (as highlighted in magenta in (a), the same area as in Figures 5 and 9 of KM2017). (c) Multimodel mean historical climatology of DJF zonal mean zonal wind (contours, contour interval = 5 m/s) and difference in multimodel mean climatology between the weakening group and strengthening group (color shadings). (d) Similar to (c) but for the linear refractive index. The contour interval = 20 for thin black contours and thick black contours highlight values of 0 and 10. The magenta cross in (c) and (d) indicates the location with negative climatological refractive index in the multimodel mean and it is located at 38°N, 70 hPa. (e and f) Similar to (b) but with DJF climatological linear refractive index and climatological zonal mean zonal wind, respectively, evaluated at the magenta cross location as in (c) and (d). Stippling in (a), (c), and (d) indicates that the changes in the two groups are statistically significantly different from each other at the 95% confidence level using two-sided Student's *t* test. In (b), (e), and (f), the blue symbols indicate the polar vortex weakening group and red for the strengthening group. The circles denote individual models and the crosses denote the multimodel mean for the weakening and strengthening groups. Correlation coefficients are indicated in the title of (b), (e), and (f), but none is statistically significant at the 95% confidence level.

The reason underlying this difference primarily lies in the difference in models and model ensemble members that are used (Figure 11b of Manzini et al., 2014, used 24 models with mostly only one run while 35 models with all available ensemble members are used in our study). Considering the larger number of models and ensembles used in our study, our results better represent the forced response and the intermodel spread among the coupled CMIP5 models. In addition, Figure 2e further shows the relationship between the climatological refractive index evaluated in the location of negative n^2_{ref} in the multimodel mean and the stratospheric polar vortex change across all the coupled CMIP5 models. No significant linear relationship is found between these two quantities. This is also true when considering the minimum n^2_{ref} in the subtropical lower stratosphere region for each model, accounting for the possibility that the negative region may occur in a different location in different models (not shown). Figure 2f is similar to Figure 2e but shows the correlation with the climatological jet strength in the location of negative n^2_{ref} and no significant relationship is found. Therefore, neither the KM2017 nor SS2010 mechanism is able to explain the intermodel spread of the stratospheric polar vortex in the coupled CMIP5 ensemble.

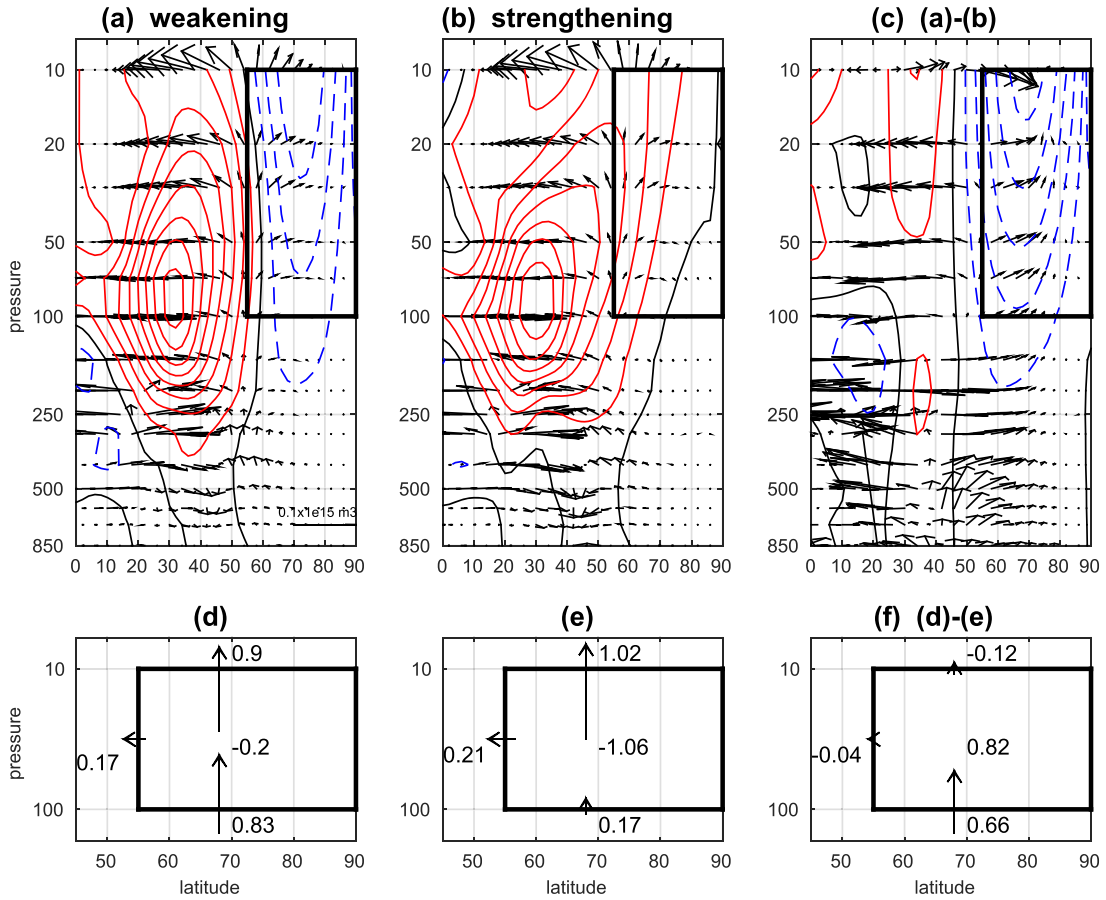

Figure 3. The change in DJF E-P flux (vectors) and JFM zonal mean zonal wind (contours) for (a) the polar vortex weakening group, (b) the polar vortex strengthening group, and (c) their difference. The E-P flux vectors are scaled according to equation (3.13) of Edmon et al. (1980), and the horizontal arrow scale (0.1×10^{15} m^3) is indicated in the bottom right corner of (a). The E-P flux vectors in (c) are scaled by a factor of 5 larger than (a) and (b). The contour interval is 1 m/s for (a)–(c) and solid red, dashed blue, and solid black contours denote positive, negative, and zero values, respectively. The change in E-P flux at the three boundaries of the stratospheric region (highlighted by thick black box in all subplots) and the change in net E-P flux convergence for (d) the polar vortex weakening group, (e) the polar vortex strengthening group, and (f) their difference. Numbers are in units of 10^4 kg m/s^4. The E-P flux change is defined as positive for upward E-P flux at 10 and 100 hPa and equatorward E-P flux at 55°N. The arrows in (d)–(f) are scaled to reflect the relative size of the contributions.

3.3. Relationship With E-P Flux Changes

Next we use the E-P flux diagnostic to further examine the stratospheric polar vortex change and its relationship with the change in stationary wave driving across models. First, Figures 3a–3c summarize the multimodel mean E-P flux change for the weakening group, the strengthening group, and their difference during DJF. As described in section 2, the region over 55°–90°N, 10–100 hPa is chosen as the stratospheric region for the E-P flux budget analysis as it encompasses the polar vortex deceleration region below 10 hPa in the weakening group as shown in Figure 3a. The multimodel mean of all CMIP5 models (Figures 3a, 3b, 3d, and 3e) shows an increase in upward E-P flux between 55°N and 90°N at both 100 and 10 hPa and an increase in equatorward E-P flux at 55°N between 100 and 10 hPa. Comparing the mean of the two groups (Figures 3c and 3f), the weakening group has more of an increase of upward E-P flux at 100 hPa, less of an increase of upward E-P flux at 10 hPa, and a smaller increase in equatorward E-P flux at 55°N, all of which contribute to an increased E-P flux convergence into the stratospheric region (0.82×10^4 kg m/s^4 in Figure 3f is statistically significant at the 95% confidence level), consistent with the greater weakening of the stratospheric polar vortex.

Considering the intermodel spread in more detail, Figure 4a shows the relationship between the stratospheric polar vortex change and net E-P flux convergence change in the stratospheric vortex region across all the CMIP5 models. As expected, a statistically significant negative correlation (−0.52) is found between the two across the 35 models, indicating that models that simulate a greater weakening of the stratospheric

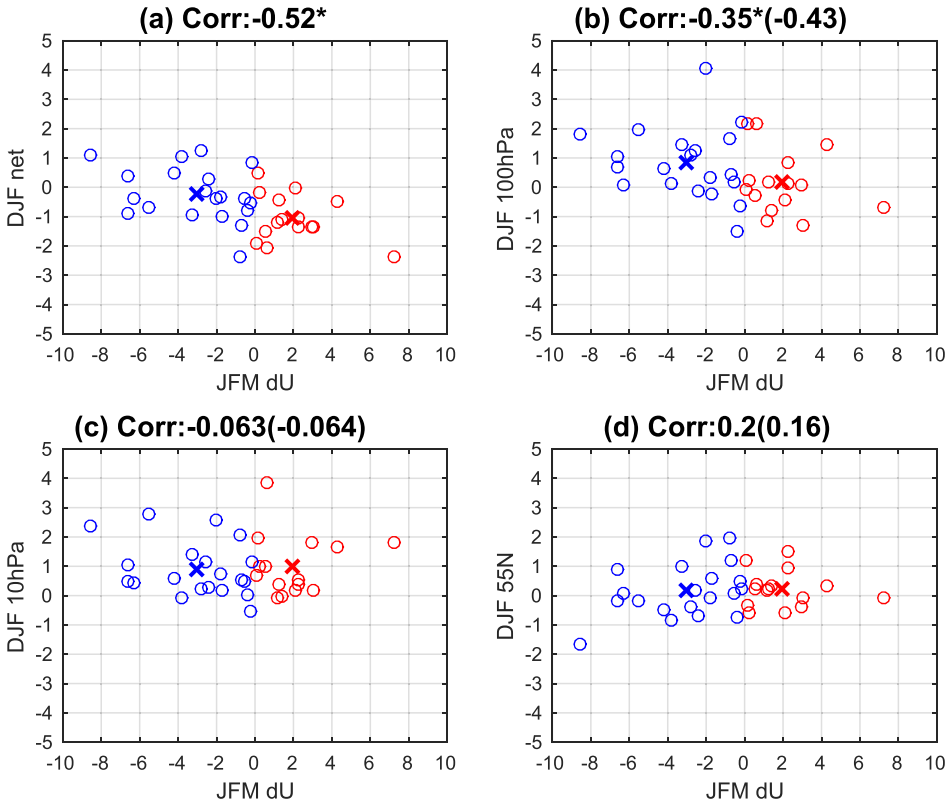

Figure 4. The relationship between the JFM stratospheric polar vortex change (in units of m/s) and the DJF net E-P flux convergence change (a), the E-P flux change across 100 hPa between 55°N and 90°N (b), across 10 hPa between 55°N and 90°N (c), and across 55°N between 100 and 10 hPa (d) (in units of 10^4 kg m/s^4) across the CMIP5 models. The correlation coefficient is indicated in the title, and the correlation coefficient weighted by the ratio of the standard deviations is indicated within the parentheses. The asterisk symbol indicates that the correlation coefficient is statistically significant at the 95% confidence level. The blue symbols indicate the polar vortex weakening group and red for the strengthening group. The circles denote individual models and the crosses denote the multimodel mean for the weakening and strengthening groups.

polar vortex are associated with a larger E-P flux convergence in this region and vice versa. However, only a small portion (27%) of the intermodel spread in the stratospheric polar vortex can be explained by this quantity. The results shown here are representative of those obtained using the polar vortex change at other latitudes and pressure levels (Figure S1b) and using the equatorward lateral boundary of the stratospheric region at 45°N (not shown). The correlation is found to be about −0.47 with the changes in zonal mean zonal wind averaged over the stratospheric region (not shown). The conclusions also remain largely the same with concurrent polar vortex change and net E-P flux convergence change (Figures S1c and S1d).

In addition, considering that both the transient and stationary eddies contribute to the full E-P flux (e.g., Figure 14.9 of Peixoto & Oort, 1992), we examine how the relationship in Figure 4a is affected when both types of eddies are included with a smaller model ensemble. Figure S2 is similar to Figure 4a but uses one member of 14 coupled CMIP5 models that have 6-hourly model-level output available. Comparing the results with 6-hourly model-level output and those with monthly pressure-level output among this 14-model ensemble, the correlation coefficients are similar (−0.57 for the former as shown in Figure S2a and −0.64 for the latter as shown in Figure S2b). Thus, including high-frequency transient eddies does not appear to help explain more of the intermodel spread in the polar vortex change than using the stationary component alone, at least in this ensemble of 14 models. Given this, we continue with the 35 CMIP5 model ensemble and monthly data for the E-P flux analysis, given the larger number of models and ensemble members available.

Following equation (5), Figures 4b–4d further shows the relationship with the E-P flux changes at the three boundaries of the stratospheric region. It can be seen that the relationship between the polar vortex

change and net E-P flux convergence change is not dominated by any single contributor but rather is contributed by changes in both the upward E-P flux at 100 hPa, and to a lesser extent, the equatorward E-P flux at 55°N. More specifically, the models that have a greater polar vortex weakening are associated with a larger increase in upward E-P flux at 100 hPa (correlation is −0.35) and less of an increase in equatorward E-P flux at 55°N (correlation is 0.2, though statistically insignificant). Also, it is notable that models disagree on the sign of the changes in E-P flux at 100 hPa and across 55°N, while there is modest agreement on increased E-P flux at 10 hPa. In addition, while the correlation coefficients themselves are not linearly additive, the correlation coefficients weighted by ratios of standard deviations are: $r(\Delta\mathrm{EPflux}_{\mathrm{net}}, \Delta\mathrm{u}) = r(\Delta\mathrm{EPflux}_{100\mathrm{hPa}}, \Delta\mathrm{u}) \times \frac{\sigma(\Delta\mathrm{EPflux}_{100\mathrm{hPa}})}{\sigma(\Delta\mathrm{EPflux}_{\mathrm{net}})} - r(\Delta\mathrm{EPflux}_{10\mathrm{hPa}}, \Delta\mathrm{u}) \times \frac{\sigma(\Delta\mathrm{EPflux}_{10\mathrm{hPa}})}{\sigma(\Delta\mathrm{EPflux}_{\mathrm{net}})} - r(\Delta\mathrm{EPflux}_{55\mathrm{N}}, \Delta\mathrm{u}) \times \frac{\sigma(\Delta\mathrm{EPflux}_{55\mathrm{N}})}{\sigma(\Delta\mathrm{EPflux}_{\mathrm{net}})}$, where r denotes correlation coefficient, σ denotes standard deviation across models, and Δ indicates the future change. As shown in Figure 4, the correlation coefficients weighted by the ratio of standard deviations, shown within the parentheses in the figure titles, can add up to the correlation between the polar vortex change and net E-P flux convergence change, that is, $-0.43 - (-0.064) - 0.16 \approx -0.52$.

Therefore, we have found that less than 30% of the intermodel spread in the stratospheric polar vortex change across the 35 CMIP5 can be explained by the change in resolved stationary wave driving in this region and this has contributions from the change in both upward and equatorward wave propagation. Given the results in Figure S2, we expect this conclusion would not change appreciably if transient wave activity were also included. The small portion of variance explained by the resolved wave driving suggests that parameterized processes, such as gravity waves, might also likely contribute to the intermodel spread of the polar vortex. It is also possible that resolved wave driving outside of the domain considered could play a role. However, these processes are hard to quantify due to the lack of model output in the CMIP5 archive.

4. Conclusion and Discussions

In this study, we have analyzed the intermodel spread of the northern winter stratospheric polar vortex change across 35 models in the fully coupled CMIP5 simulations under RCP8.5 forcing and found that:

1. Neither of the two prevailing hypotheses (i.e., Karpechko & Manzini, 2017; Sigmond & Scinocca, 2010) is able to explain the intermodel spread of the stratospheric polar vortex among the coupled CMIP5 simulations.
2. The resolved stationary wave driving in the region between 100 and 10 hPa and 55°N and the pole accounts for less than 30% of the intermodel spread of the stratospheric polar vortex change, and both the vertical wave propagation from the troposphere into the stratosphere and the horizontal wave propagation within the stratosphere contribute to the intermodel difference in the wave driving. In addition, this percentage of variance is not significantly altered by including the high-frequency transient eddies in a subset of models.

Although a month of lead-lag is included to assess the wave drag conditions prior to the stratospheric polar vortex change and is typically used in previous studies, we caution that the tropospheric anomalies associated with the stratospheric anomalies could be both response and forcing to the stratospheric anomalies. For example, the difference in multimodel mean eddy geopotential height change between the weakening and the strengthening groups shows a high anomaly over the North Atlantic. However, this also resembles the downward influence of the stratospheric polar vortex weakening on the troposphere (e.g., see Figure 6e of Simpson et al., 2018). Therefore, it is challenging to disentangle response and forcing in the coupled stratosphere-troposphere system in the CMIP5 archive and doing so requires targeted experiments.

We have performed our analysis by using all available ensemble members in order to minimize the role played by internal variability of the stratospheric polar vortex. However, we note that even when all members are used, internal variability could still play a role in contributing to the intermodel spread. As found in Simpson et al. (2018), roughly half of the models exhibit a change in vortex strength that is not greater than expected to arise from the sampling of internal variability while the remaining models on both the extreme weakening and strengthening ends of the distribution do exhibit a significant response (see their Figure 1e). Our analysis, therefore, includes both models where the change in vortex strength is large and significant, and those where it is not greater than expected to arise from the sampling of internal variability.

We have shown that less than 30% of the intermodel spread of the stratospheric polar vortex change among the 35 CMIP5 models can be explained by the resolved stationary wave driving in the region between 100 and

10 hPa and 55°N and the pole. Parameterized processes such as gravity waves as well as resolved waves outside of the region considered might also contribute to the intermodel spread but their contributions are hard to assess because of the lack of relevant model output. There is hope that a more detailed budget analysis can be made through the Dynamics and Variability Model Intercomparison Project in CMIP6, in which an enhanced archive of variables and diagnostics will be available for analysis of both resolved and parameterized processes underlying the modeled dynamics (Gerber & Manzini, 2016). More specifically, diagnostics such as daily tendencies of eastward wind due to E-P flux divergence, nonorographic and orographic gravity waves, Transformed Eulerian Mean (TEM) northward wind advection and the Coriolis term, and TEM upward wind advection will be made available on a wider range of vertical levels, which would allow a better closure of the zonal wind tendency equation and a detailed budget analysis as well as the contribution of the wave driving outside of the domain considered here.

In summary, the intermodel spread of the stratospheric polar vortex response to climate change does not appear to be dominated by any single mechanism and current proposed theories appear inadequate to explain the spread. We caution that hypotheses developed using a limited number of models or idealized scenarios are not necessarily applicable when it comes to explaining the overall spread in the fully coupled CMIP5 simulations. Since the stratospheric polar vortex plays an important role in climate processes, including at the surface, this motivates efforts to improve understanding of changes in the detailed budget of the stratospheric circulation by including both resolved and parameterized waves and how they interact with the mean flow. This also highlights a need for an improved theoretical understanding underlying the changes in both horizontal and vertical wave propagation and the stratospheric polar vortex response to climate change.

Acknowledgments
This work was supported by NSF Award AGS-1317469. The authors thank the reviewers for their constructive comments and suggestions. The authors also would like to thank the support from the research staff at the Ocean and Climate Physics Division of the Lamont-Doherty Earth Observatory. Y. W. would like to thank Xinyue Wang for her help with some of the CMIP5 data. The authors acknowledge the World Climate Research Programme's Working Group on Coupled Modelling, which is responsible for CMIP, and we thank the climate modeling groups for producing and making available their model output. For CMIP the U.S. Department of Energy's Program for Climate Model Diagnosis and Intercomparison provides coordinating support and led development of software infrastructure in partnership with the Global Organization for Earth System Science Portals. The CMIP5 data used in this study are freely available through the Earth System Grid Federation (https://esgf-node.llnl.gov).

References

Edmon, H. J., Hoskins, B. J., & McIntyre, M. E. (1980). Eliassen-Palm cross sections for the troposphere. *Journal of the Atmospheric Sciences*, *37*, 2600–2616. https://doi.org/10.1175/1520--0469(1980)037,_2600:EPCSFT.2.0.CO;2

Gerber, E. P., Butler, A., Calvo, N., Charlton-Perez, A., Giorgetta, M., Manzini, E., et al. (2012). Assessing and understanding the impact of stratospheric dynamics and variability on the Earth system. *Bulletin of the American Meteorological Society*, *93*, 845–859. https://doi.org/10.1175/BAMS--D--11--00145.1

Gerber, E. P., & Manzini, E. (2016). The Dynamics and Variability Model Intercomparison Project (DynVarMIP) for CMIP6: Assessing the stratospheretroposphere system. *Geoscientific Model Development*, *9*, 3413–3425. https://doi.org/10.5194/gmd--9--3413--2016

Hu, Y., & Tung, K. K. (2002). Interannual and decadal variations of planetary wave activity, stratospheric cooling, and Northern Hemisphere Annular Mode. *Journal of Climate*, *15*, 1659–1673. https://doi.org/10.1175/1520–0442(2002)015lt;1659:IADVOP>2.0.CO;2

Karpechko, A. Y., & Manzini, E. (2017). Arctic stratosphere dynamical response to global warming. *Journal of Climate*, *30*, 7071–7086. https://doi.org/10.1175/JCLI--D--16--0781.1

Kidston, J., Scaife, A. A., Hardiman, S. C., Mitchell, D. M., Butchart, N., Baldwin, M. P., & Gray, L. J. (2015). Stratospheric influence on tropospheric jet streams, storm tracks and surface weather. *Nature Geoscience*, *8*, 433–440. https://doi.org/10.1038/NGEO2424

Kushner, P. J., & Polvani, L. M. (2004). Stratospheretroposphere coupling in a relatively simple AGCM: The role of eddies. *Journal of Climate*, *17*, 629–639. https://doi.org/10.1175/1520–0442(2004)017lt;0629:SCIARS>2.0.CO;2

Manzini, E., Karpechko, A. Y., Anstey, J., Baldwin, M. P., Black, R. X., Cagnazzo, C., et al. (2014). Northern winter climate change: Assessment of uncertainty in CMIP5 projections related to stratospheretroposphere coupling. *Journal of Geophysical Research: Atmospheres*, *119*, 7979–7998. https://doi.org/10.1002/2013JD021403, .

Peixoto, J. P., & Oort, A. H. (1992). *Physics of climate* (1st ed.). New York: American Institute of Physics. February 1, 1992.

Scaife, A. A., Spangehl, T., Fereday, D. R., Cubasch, U., Langematz, U., Akiyoshi, H., et al. (2012). Climate change projections and stratosphere-troposphere interaction. *Climate Dynamics*, *38*, 2089–2098. https://doi.org/10.1007/s00382--011--1080--7

Shindell, D. T., Miller, R. L., Schmidt, G. A., & Pandolfo, L. (1999). Simulation of recent northern winter climate trends by greenhouse-gas forcing. *Nature*, *399*, 452–455. https://doi.org/10.1038/20905

Sigmond, M., & Scinocca, J. F. (2010). The influence of the basic state on the Northern Hemisphere circulation response to climate change. *Journal of Climate*, *23*, 1434–1446. https://doi.org/10.1175/2009JCLI3167.1

Simpson, I. R., Hitchcock, P., Seager, R., Wu, Y., & Callaghan, P. (2018). The downward influence of uncertainty in the Northern Hemisphere stratospheric polar vortex response to climate change. *Journal of Climate*, *31*, 6371–6391. https://doi.org/10.1175/JCLI--D--18--0041.1

Zappa, G., & Shepherd, T. G. (2017). Storylines of atmospheric circulation change for European regional climate impact assessment. *Journal of Climate*, *30*, 6561–6577. https://doi.org/10.1175/JCLI--D--16--0807.1